RSC Medicinal Chemistry

ROYAL SOCIETY OF CHEMISTRY

RESEARCH ARTICLE

View Article Online
View Journal | View Issue

Check for updates

Cite this: *RSC Med. Chem.*, 2025, **16**, 2133

# Nitroreductase-activatable photosensitizers for selective antimicrobial photodynamic therapy†

Matthew T. Tung,[ab] Tianyi Ma,[ac] Ivonne Rebeca Lopez-Miranda,[ab] Joshua N. Milstein *[ac] and Andrew A. Beharry *[ab]

Received 13th November 2024,
Accepted 16th February 2025

DOI: 10.1039/d4md00890a

rsc.li/medchem

Antimicrobial photodynamic therapy (aPDT) utilizes light, oxygen and a photosensitizer (PS) to enact cell death *via* the production of reactive oxygen species (ROS). This mechanism of cell death, *via* oxidative stress, has allowed aPDT to be effective against antibiotic-resistant bacterial strains, with the development of resistance being minimal as no specific pathway is targeted. While promising, as ambient light can activate PSs, damage to mammalian tissues can occur, leading to drug-induced photosensitivity. To mitigate this, we developed a nitroreductase-activatable PS containing a quenching group that inhibits fluorescence and ROS. Upon reaction with nitroreductase, the quenching group can be liberated, restoring fluorescence and ROS production. As nitroreductase is not present in healthy mammalian tissues but expressed in many bacteria, photosensitivity of mammalian cells can be reduced. Herein, the synthesis and photophysical characterization of the nitroreductase-activatable PS, **DB2**, is described. **DB2** was quenched compared to the free PS, **DB1**, and activation both *in vitro* by purified nitroreductase and in the gram-positive bacterial strain, *Bacillus subtilis*, was confirmed by fluorescence recovery. Cell viability studies in *B. subtilis* showed low dark toxicity and an $IC_{50}$ of 0.16 μM under 10-minute irradiation (530 nm, 42 mW $cm^{-2}$). Minimal toxicity was observed under the same conditions in mammalian cell cultures demonstrating the potential of **DB2** to mitigate photosensitivity and provide a promising approach for aPDT.

Open Access Article. Published on 06 March 2025. Downloaded on 5/10/2026 2:26:02 AM.
This article is licensed under a Creative Commons Attribution-NonCommercial 3.0 Unported Licence.

With the constant use of antibiotics to treat infections, antimicrobial resistance (AMR) continues to rise, and it is estimated that over 10 million deaths per year will be caused by AMR by 2050.[1] To combat this trend, alternative treatments such as antimicrobial photodynamic therapy (aPDT) are being developed. Antimicrobial PDT is a subset of PDT, a clinically approved cancer treatment requiring light, oxygen and a chromophore photosensitizer (PS).[2–4] Upon irradiation with light, a PS can absorb the incoming photon entering an excited singlet state. From here, the PS can undergo intersystem crossing into an excited triplet state where they interact with nearby biomolecules and oxygen to generate cytotoxic reactive oxygen species (ROS), such as singlet oxygen ($^1O_2$), leading to cell death *via* oxidative stress.[2–4] Additionally, some PSs can relax from the singlet excited state to the ground state *via* fluorescence, enabling detection. For aPDT, bacteria, fungi, viruses and protozoa are targeted instead of cancerous tissues and can provide certain advantages over traditional antibiotics as the generation of ROS invokes cell death by a different mechanism (*i.e.* oxidative stress).[5–7] Therefore, aPDT has been demonstrated to be effective against antibiotic-resistant bacterial strains and, as no specific enzyme or pathway is targeted, the development of resistance in bacteria is also slower when compared to the usage of antibiotics.[5–7] This has led to the development of many PSs for aPDT summarized in numerous review articles.[8–10] Although a promising strategy, aPDT can have adverse side effects as PSs can accumulate in healthy mammalian tissues. This may cause unwanted cell damage and death leading to photosensitivity in patients.[8–10]

Cationic PSs have demonstrated higher efficacy towards bacteria,[10–12] and PS-conjugates to antibiotics,[13–15] nanoparticles,[16–18] and peptides[19,20] are being developed to promote permeability into bacteria. However, in both cases, the PS is always in an "ON" state, whereby ambient light can activate the PS, leading to photosensitivity. To mitigate this, compounds containing quenched PSs, known as activatable PSs (aPSs), are being pursued. By introducing an enzyme-

[a] *Department of Chemical & Physical Sciences, University of Toronto Mississauga, 3359 Mississauga Road North, Mississauga, Ontario L5L 1C6, Canada*
[b] *Department of Chemistry, University of Toronto, 80 St. George Street, Toronto, Ontario M5S 3H6, Canada. E-mail: andrew.beharry@utoronto.ca*
[c] *Department of Physics, University of Toronto, 60 St. George Street, Toronto, Ontario M5S 1A7, Canada. E-mail: josh.milstein@utoronto.ca*

† Electronic supplementary information (ESI) available: Photophysical characterizations of all compounds, including extinction coefficient graphs, *in vitro* assays, *E. coli* experiments with **DB2**, images of colony formation for *B. subtilis* treatments, synthetic scheme for **EY2**, $^1H$ and $^{13}C$ NMR spectra, and MS data. See DOI: https://doi.org/10.1039/d4md00890a

Open Access Article. Published on 06 March 2025. Downloaded on 5/10/2026 2:26:02 AM.
This article is licensed under a Creative Commons Attribution-NonCommercial 3.0 Unported Licence.

activatable trigger group that can also quench the PS, aPSs are effectively in an "OFF" state producing low levels of fluorescence and ROS production when irradiated.[21,22] Upon reaction with the target enzyme, the trigger group can be cleaved liberating a free PS in its "ON" state and recovering its fluorescence and ROS production.[21,22] As a result, only cells (*i.e.* bacteria) that express the target enzyme can activate the aPS and generate sufficient ROS upon irradiation to enact cell death. Non-targeted cells (*i.e.* mammalian cells) will contain the inactive aPS producing less ROS and, therefore, minimize photosensitivity. As fluorescence is also quenched for aPSs, this method can also be used to diagnose the presence of the targeted cells, when activated, and to verify specificity.[21,22]

To develop an aPS selectively for aPDT, nitroreductase (NTR), an enzyme capable of reducing nitro groups into amines using nicotinamide adenine dinucleotide (NADH) as a cofactor, was chosen for two reasons. First, NTR is expressed in many bacterial strains such as *Escherichia coli*, *Staphylococcus aureus*, and *Bacillus subtilis*, while not being expressed in healthy mammalian cells.[23] This has led to NTR prodrugs[24,25] and NTR-activated fluorophores[26,27] being used for the treatment and diagnostics of bacteria. Secondly, NTR can interact with the 4-nitrobenzyl trigger group, a known fluorescence and ROS quencher. By tethering 4-nitrobenzyl onto a PS, we reasoned that the NTR-aPSs would have low fluorescence and ROS production until reaction with NTR (Fig. 1), thereby providing higher selectivity when compared to using a PS alone. It should be noted that NTR can also be expressed in the hypoxic, low-oxygen environments commonly found within tumours, which has led to many NTR-aPSs being synthesized and tested for PDT applications.[28,29] However, to our knowledge, studies using aPSs for aPDT are limited and only one known exploiting NTR has been reported, which used a hemicyanine-based PS that had a low singlet oxygen quantum yield and targeted intracellular bacteria.[22] Herein, the synthesis and photophysical characterization of **DB2**, a fluorescein-based NTR-aPS are described. Fluorescein-based PSs can have high singlet oxygen and fluorescence quantum yields. By appending the 4-nitrobenzyl group onto 4′,5′-dibromofluorescein (DBFCN), a known PS, the fluorescence and ROS production is quenched. After incubation with purified NTR and NADH, cleavage of the trigger group was observed by the release of the fluorescent product. Bacterial cell studies were then conducted in the gram-positive *Bacillus subtilis* model strain where **DB2** demonstrated activation and managed to kill cells with an absolute $IC_{50}$ value of 0.16 μM with 10 minutes of irradiation (530 nm, 41.8 mW $cm^{-2}$). With the broad number of bacterial strains that express NTR, and the rising health concerns caused by AMR bacteria, the development of novel NTR-aPSs such as **DB2** can further build upon the foundation for aPDT.

## Results and discussion

The synthesis of **DB2** proceeded in two steps starting with commercially available DBFCN (Scheme 1). To direct the 4-nitrobenzyl group towards the hydroxyl on the xanthene core, the first step involved protecting the carboxylic acid with a methyl group forming a methyl ester, **DB1**. Nucleophilic substitution of DB1 to nitrobenzyl bromide yielded **DB2**. All $^{1}H$ and $^{13}C$ NMR and MS data can be seen in the supplementary information.

To determine **DB2**'s potential as an NTR-aPS, the photophysical properties were determined and compared to **DB1**, the expected product from the NTR reaction (Fig. 1). All photophysical characterizations were conducted using DMSO stocks of the respective compounds diluted in phosphate buffered saline (PBS) to a final concentration containing 2% DMSO unless otherwise specified. The absorbance of **DB1** showed a slight redshift of 5 nm ($\lambda_{abs}$ = 508 nm) compared to DBFCN. With the addition of the 4-nitrobenzyl group, the absorbance of **DB2** showed peak broadening with a significant 38 nm blueshift ($\lambda_{abs}$ = 470 nm) (Fig. 2a). To monitor fluorescence quenching, the absorbances of the compounds were matched at 0.1 AU at 503 nm and fluorescence spectra were obtained (Fig. 2b), showcasing that **DB2** has lower fluorescence than **DB1**. To further confirm the quenching capabilities of the 4-nitrobenzl group, the fluorescence quantum yields ($\Phi_f$) were then obtained in PBS. **DB2** was ~11-fold quenched compared to **DB1** (0.024 ± 0.002 and 0.26 ± 0.01 for **DB2** and **DB1**, respectively, using Rhodamine B ($\Phi_f$ = 0.5 in ethanol)[30] as a standard, confirming that the 4-nitrobenzyl group acts as a quencher. The singlet oxygen quantum yields ($\Phi_\Delta$) were then measured using 9,10-anthracenediyl-bis(methylene)dimalonic acid (ABDA), a selective $^{1}O_2$ sensor that decreases in absorbance at 401 nm upon reaction with $^{1}O_2$. Consistent with fluorescence quenching, **DB2** was ~2-fold quenched compared to **DB1** ($\Phi_\Delta$ = 0.38 ± 0.04 and 0.20 ± 0.02

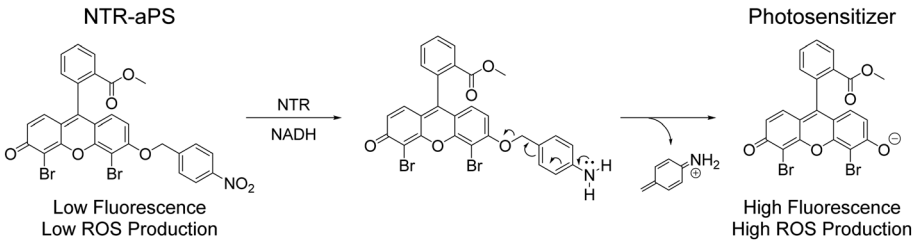


**Fig. 1** Mechanism of action for NTR-aPSs. Upon reaction with NTR, the nitro group is reduced to an amine, leading to cleavage and the release of the free PS.

 This journal is © The Royal Society of Chemistry 2025

Open Access Article. Published on 06 March 2025. Downloaded on 5/10/2026 2:26:02 AM.
This article is licensed under a Creative Commons Attribution-NonCommercial 3.0 Unported Licence.

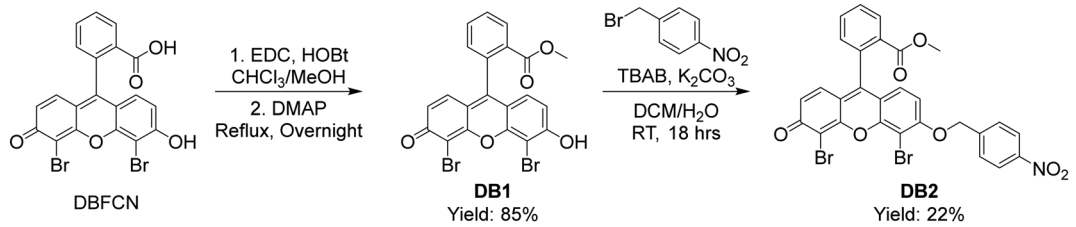


**Scheme 1** Synthesis of **DB2**. The carboxylic acid on DBFCN is converted to a methyl ester in the first step to direct nucleophilic substitution of the 4-nitrobenzyl group towards the hydroxyl group in the subsequent step.

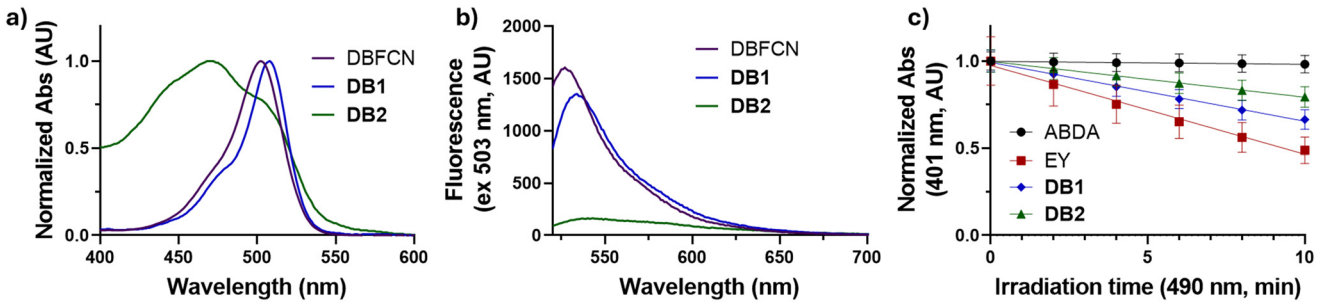


**Fig. 2** Photophysical characterizations of **DB2** in PBS (2% DMSO). (a) Normalized absorbance spectra of compounds. (b) Fluorescence spectra of compounds. (c) $^1O_2$ generation of compounds monitored by the absorbance of ABDA at 401 nm under 490 nm irradiation (28.0 mW cm$^{-2}$). EY was chosen as the standard and ABDA under irradiation serves as a control. Experiments were conducted in triplicate.

for **DB1** and **DB2** respectively) (Fig. 2c) using Eosin Y (EY) as a control ($\Phi_\Delta$ = 0.50 in $H_2O$)[31] under irradiation at 490 nm (28.0 mW cm$^{-2}$).

With the quenching of fluorescence and ROS generation observed in **DB2** compared to **DB1**, the extinction coefficients ($\varepsilon$) were determined in DMSO by quantitative NMR (Fig. S1†) at their respective $\lambda_{abs}$ in DMSO (Fig. S2†) and used to determine the concentrations for subsequent experiments. The difference in $\varepsilon$ between the two compounds can further enhance the quenching observed as **DB2** has a significantly lower $\varepsilon$ (1,700 M$^{-1}$ cm$^{-1}$) compared to **DB1** (123 000 M$^{-1}$ cm$^{-1}$) when compared at 531 nm in DMSO. All photophysical properties are summarized in Table 1.

To confirm that NTR can recognize **DB2** and release **DB1**, an *in vitro* fluorescence time-course assay was conducted. Upon incubating purified NTR, NADH, and **DB2**, the fluorescence increased over the 10-minute incubation period in contrast to a sample containing only NADH and **DB2** (Fig. 3a). The fluorescence spectra before and after the incubation were also obtained (Fig. 3b) and the $\lambda_{em}$ matched that of **DB1**. To further confirm the release of **DB1**, the $\lambda_{abs}$ of the product after incubation also matched **DB1** with a similar peak shape showcasing its release (Fig. 3c). The increase in absorbance observed after activation also highlights the additional quenching caused by the change in ε between the two compounds. No changes in fluorescence and absorbance were observed upon incubating **DB2** in the absence of NTR (Fig. S3†).

With this promising *in vitro* data, **DB2** was incubated separately with two NTR-containing model bacteria, *Bacillus subtilis* (Gram-positive strain) and *Escherichia coli* (Gram-negative strain), to monitor the release of **DB1** *via* observing the fluorescence increase over time. Utilizing an initial optical density ($OD_{600}$) of 0.05 AU at 600 nm for both bacterial strains, 1 μM of **DB2** was incubated independently with both strains and compared to controls with bacteria only and **DB2** only for 24 hours. As seen in Fig. 4a, *B. subtilis* showed a fluorescence increase suggesting activation and release of the free PS, **DB1**. However, no substantial difference in fluorescence was observed with *E. coli* (Fig. S4†), which we attributed to the permeability barrier formed by the dual cell membrane of *E. coli* preventing entry of **DB2**.[32] Therefore, *B. subtilis* was chosen for further experiments to determine if **DB2** can enact bacterial cell death.

Utilizing an initial $OD_{600}$ of 0.05, a variety of concentrations of **DB2** were incubated with *B. subtilis* at room temperature for 4 hours and left in the dark or irradiated at 530 nm for 10 minutes (41.8 mW cm$^{-2}$). The $OD_{600}$ of the dark control (*B. subtilis* only) was then measured to calculate the dilution factor required to reach a final $OD_{600}$ of 2.5 × 10$^{-4}$ for plating. All

**Table 1** Summary of the photophysical data for **DB1** and **DB2**

| | DB1 | DB2 |
|---|---|---|
| $\lambda_{abs}$ (nm, PBS) | 507 | 470 |
| $\lambda_{em}$ (nm, PBS) | 534 | 537 |
| $\lambda_{abs}$ (nm, DMSO) | 531 | 464 |
| $\varepsilon$ (M$^{-1}$ cm$^{-1}$, DMSO)[a] | 123 000 | 39 000 |
| $\Phi_f$ (PBS) | 0.26 ± 0.01 | 0.024 ± 0.002 |
| $\Phi_\Delta$ (PBS) | 0.38 ± 0.04 | 0.20 ± 0.02 |

[a] Extinction coefficients were determined at the respective maximum $\lambda_{abs}$ in DMSO.

Open Access Article. Published on 06 March 2025. Downloaded on 5/10/2026 2:26:02 AM.
This article is licensed under a Creative Commons Attribution-NonCommercial 3.0 Unported Licence.

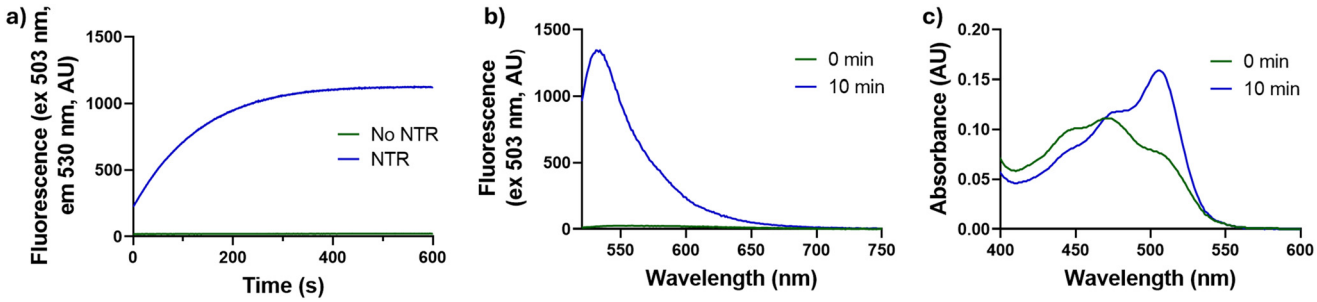


Fig. 3 Nitroreductase reaction with **DB2** in PBS (2% DMSO). (a) Fluorescence time-course of **DB2** with NTR and NADH. (b) Fluorescence spectra of **DB2** before and after 10-minute incubation with NTR and NADH. (c) Absorbance spectra of **DB2** before and after 10-minute incubation with NTR and NADH.

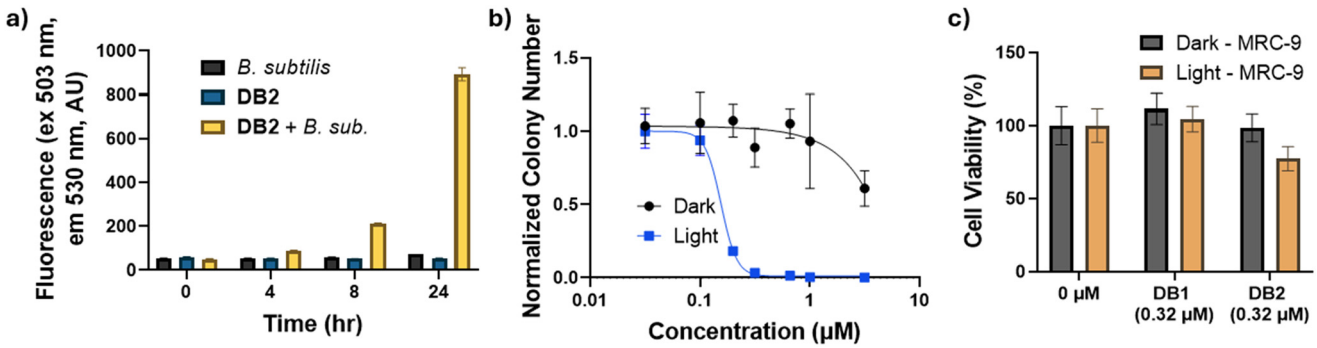


Fig. 4 Cell experiments with **DB2**. (a) Activation of **DB2** in *B. subtilis* monitored by fluorescence. Experiments were conducted in triplicate. (b) Cell viability curve of **DB2** with *B. subtilis* under dark or light conditions (10 minutes, 530 nm, 41.8 mW $cm^{-2}$). Experiments were conducted in triplicate. (c) Cell viability of **DB1** and **DB2** in MRC-9 cells under dark or light conditions (10 minutes, 530 nm, 41.8 mW $cm^{-2}$). Experiments were conducted in triplicate.

samples were diluted with LB broth, plated into 6-well plates containing agarose, and spread evenly with glass beads. The plates were incubated overnight at 37 °C and then the colonies were counted to assess cell viability (Fig. S5†). **DB2** gave an absolute $IC_{50}$ value of 0.16 μM under the irradiation conditions with dark toxicity being observed in concentrations >3.2 μM demonstrating its dependence on light and its potential for antimicrobial PDT (Fig. 4b).

Furthermore, **DB2** was tested in MRC-9 fibroblast cells, a normal lung cell line, to determine if toxicity would be observed in mammalian cells under normoxic (21% oxygen) conditions. The MRC-9 cells were incubated for four hours with **DB2** (0 or 0.32 μM) and treated under dark or the same irradiation conditions (530 nm, 41.8 mW $cm^{-2}$). A thiazolyl blue tetrazolium bromide (MTT) assay was used to assess cell viability, and no toxicity was observed in the mammalian cells under dark conditions. A mild decrease in cell viability (77 ± 8% survival) was observed in cells containing **DB2** and under irradiation (Fig. 4c) but when compared to the cell viability of *B. subtilis* under the same concentration and irradiation conditions (3.5 ± 0.8% survival), a difference of 21-fold can be seen. This is comparable to other antimicrobial techniques and showcases the selectivity **DB2** has towards targeting bacteria compared to mammalian cells.[33] We also tested DB1 under the same conditions and observed no light or dark toxicity. Since DB1 contains not NTR trigger group, we hypothesize its lack of light-dependent toxicity may be due to poor cell permeability. Similar results with DB2 were also obtained in the mammalian, HeLa cervical cancer cell line (Fig. S6†),

To demonstrate that NTR expression aids **DB2** in causing bacterial cell death, the compound **EY2** was synthesized using similar synthetic procedures as **DB2** except EY served as the base PS (Fig. 5a, Scheme S1†). EY was chosen due to the similarities it has with DBFCN except, instead of having two bromines, EY contains four. Therefore, it was hypothesized that the extra steric bulk around the ether bond would hinder the recognition of the 4-nitrobenzyl group by NTR making **EY2** unable to be activated. *In vitro* experiments were conducted and **EY2** exhibited similar photophysical properties to **DB2** (Fig. S7–S9, Table S1†). However, when incubating **EY2** with purified NTR, no fluorescence recovery was observed (Fig. S10†) demonstrating the inability of NTR to recognize **EY2**. Furthermore, when **EY2** was incubated with *B. subtilis*, no substantial fluorescence was observed until 8 hours (Fig. 5b). Finally, the cell viability of *B. subtilis* was tested under the same conditions with **EY2** and less cell death was observed compared to **DB2** showcasing the dependence of NTR and, generally, that activation of the aPS can lead to improvements in $IC_{50}$ values.

 This journal is © The Royal Society of Chemistry 2025

Open Access Article. Published on 06 March 2025. Downloaded on 5/10/2026 2:26:02 AM.
This article is licensed under a Creative Commons Attribution-NonCommercial 3.0 Unported Licence.

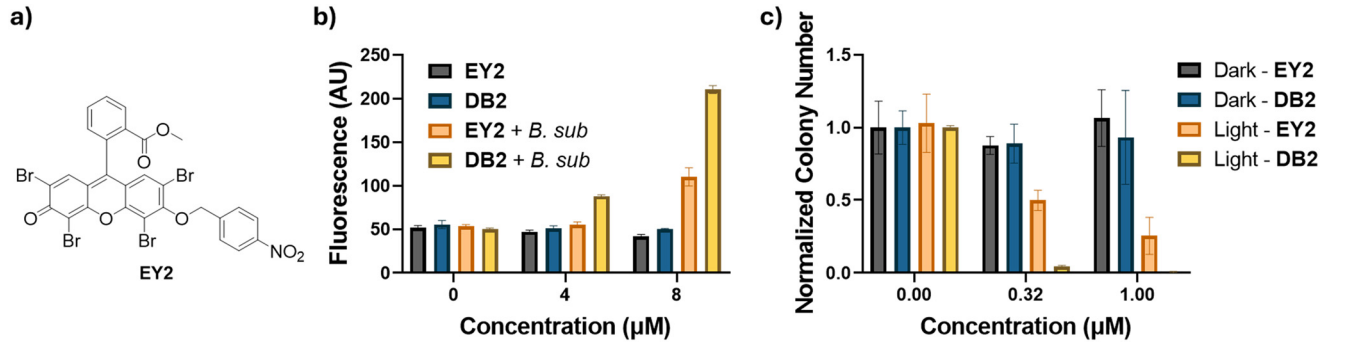


Fig. 5 Cell experiments with **EY2** control. (a) Structure of **EY2**. (b) Activation of **EY2** in *B. subtilis* monitored by fluorescence and compared with **DB2**. Experiments were conducted in triplicate. (c) Cell viability of **EY2** in *B. subtilis* under dark or light conditions (10 minutes, 530 nm, 41.8 mW $cm^{-2}$) compared with **DB2**. Experiments were conducted in triplicate.

## Conclusion

By utilizing DBFCN as the base PS and appending the 4-nitrobenzyl trigger group, the NTR-aPS **DB2** was designed and synthesized. The fluorescence and ROS production of **DB2** is effectively in an "OFF" state, with lower $\Phi_f$ (0.024 ± 0.002) and $\Phi_\Delta$ (0.20 ± 0.02), relative to **DB1** ($\Phi_f$ = 0.26 ± 0.01, $\Phi_\Delta$ = 0.38 ± 0.04), which is the product of the NTR reaction. When incubating with purified NTR enzyme, **DB2** demonstrated a release of **DB1**, monitored by fluorescence recovery, showcasing activation and turning the probe "ON". Although **DB2** did not show activation in gram-negative *E. coli*, likely due to an inability to penetrate the cell envelope, fluorescence recovery was observed in gram-positive *B. subtilis* indicating internalization and activation of the compound. In *B. subtilis*, **DB2** demonstrated an absolute $IC_{50}$ value of 0.16 μM with dark toxicity being observed at >0.32 μM. In MRC-9 cells, **DB2** once again demonstrated low dark toxicity and had a cell viability of 77 ± 8%, showcasing a 21-fold difference compared to *B. subtilis* treated under the same conditions. Finally, **EY2** was synthesized as a control to mimic **DB2** that could not be recognized by NTR. Under the same conditions, **EY2** was unable to be activated and demonstrated lower efficacy in killing *B. subtilis*, showcasing the potential of using aPSs.

Future works include testing **DB2** against clinically relevant gram-positive bacterial strains such as *Staphylococcus aureus*[34,35] and in bacterial biofilms to mimic disease models more accurately.[36,37] The synthesis of **DB2** with different NTR trigger groups such as 5-nitrothiophene and 5-nitrofuran can also be pursued.[38] By varying the trigger group, the fluorescence and ROS quenching, permeability into cells, and the time scale for activation with NTR can be altered, which may lead to more effective NTR-aPSs. Overall, the development of **DB2** further validates the use of aPSs for aPDT to mitigate photosensitivity and provide a solution to the rising trend in AMR.

## Methods

### Synthetic materials and instrumentation

All chemicals and solvents were purchased from commercial suppliers and used without further purification. $^1$H NMR spectra were obtained using a Bruker 400 MHz NMR spectrometer while $^{13}$C NMR spectra were obtained using a 500 MHz Agilent DD2 NMR spectrometer. High-resolution mass spectroscopy (HRMS) was obtained using the Agilent 6538 UHD. Cell lines, MRC-9 and HeLa were purchased from ATCC.

### Synthesis of DB1

4′,5′-Dibromofluorescein (123 mg, 0.25 mmol) was dissolved in a 2 : 1 mixture of $CHCl_3$ and MeOH (15 mL). 1-Ethyl-3-(3-dimethyllaminopropyl)carbodiimide hydrochloride (48 mg, 0.25 mmol) and hydroxy-benzotriazole (34 mg, 0.25 mmol) were stirred at room temperature for 30 minutes. 4-(Dimethylamino)pyridine (122 mg, 1 mmol) was added and refluxed overnight at 65 °C. The reaction was then evaporated under vacuum and purified by silica chromatography (100% DCM to DCM/MeOH 90 : 10) to yield an orange solid (107 mg, 85% yield). $^1$H NMR (400 MHz, DMSO) $\delta$ 8.23 (d, $J$ = 7.8 Hz, 1H), 7.91–7.75 (m, 2H), 7.51 (d, $J$ = 7.5 Hz, 1H), 6.90–6.75 (m, 4H), 3.59 (s, 3H). $^{13}$C NMR (126 MHz, DMSO) $\delta$ 165.11, 151.32, 133.59, 133.24, 130.74, 130.70, 130.26, 129.33, 128.96, 115.49, 52.40. HRMS (ESI-MS): calculated for $C_{21}H_{12}Br_2O_5$ ([M − H]$^-$) = 500.8973 Da, found 500.8971 Da.

### Synthesis of DB2

**DB1** (100 mg, 0.2 mmol), 4-nitrobenzyl bromide (172.8 mg, 0.8 mmol), and tetrabutylammonium bromide (129 mg, 0.4 mmol) were dissolved in DCM (5 mL). $K_2CO_3$ (55.3 mg, 0.4 mmol) was dissolved in water (5 mL) and added to the above solution. The reaction was then stirred vigorously for 18 hours at room temperature. The reaction was then extracted with DCM and brine. The organic layer was dried with sodium sulphate, filtered, and evaporated under vacuum before purification by silica chromatography (100% DCM to DCM/MeOH 98 : 2) to yield an orange solid (28 mg, 22% yield). $^1$H NMR (400 MHz, DMSO) $\delta$ 8.31 (d, $J$ = 8.5 Hz, 2H), 8.25 (d, $J$ = 7.8 Hz, 1H), 7.94–7.75 (m, 4H), 7.52 (d, $J$ = 7.5 Hz, 1H), 7.25 (d, $J$ = 9.1 Hz, 1H), 6.99 (d, $J$ = 9.0 Hz, 1H), 6.87 (d, $J$ = 9.8 Hz, 1H), 6.60 (d, $J$ = 9.7 Hz, 1H), 5.55 (s, 2H), 3.60 (s, 3H). $^{13}$C NMR (126 MHz, DMSO) $\delta$ 177.51, 165.11, 158.81,

Open Access Article. Published on 06 March 2025. Downloaded on 5/10/2026 2:26:02 AM. This article is licensed under a Creative Commons Attribution-NonCommercial 3.0 Unported Licence.

154.78, 150.61, 149.55, 147.28, 143.52, 133.39, 133.35, 130.84, 130.73, 130.41, 130.05, 129.32, 128.29, 123.80, 117.73, 116.22, 111.28, 102.20, 99.37, 69.86, 52.44. HRMS (ESI-MS): calculated for $C_{28}H_{17}Br_2NO_7$ ($[M + H]^+$) = 637.9450 Da, found 637.9435 Da.

### Synthesis of EY1

Synthesized using procedures for **DB1**, the compound was an orange-red solid (92% yield). $^1$H NMR (400 MHz, DMSO) $\delta$ 8.21 (d, $J$ = 7.8 Hz, 1H), 7.85 (dt, $J$ = 32.8, 7.6 Hz, 2H), 7.51 (d, $J$ = 7.5 Hz, 1H), 7.00 (s, 2H), 3.61 (s, 3H). $^{13}$C NMR (126 MHz, DMSO) $\delta$ 165.16, 152.48, 151.02, 133.24, 133.08, 130.79, 130.68, 130.45, 129.58, 129.52, 128.40, 123.60, 112.49, 99.83, 52.47. HRMS (ESI-MS): calculated for $C_{21}H_{10}Br_4O_5$ ($[M - H]^-$) = 656.7183 Da, found 656.7172 Da.

### Synthesis of EY2

Synthesized using procedures for **DB1**, the compound was a red solid (24% yield). $^1$H NMR (400 MHz, DMSO) $\delta$ 8.31 (m, 3H), 7.98–7.83 (m, 4H), 7.53 (d, $J$ = 8.2 Hz, 1H), 7.33 (s, 1H), 7.20 (s, 1H), 5.33 (s, 2H), 3.65 (s, 3H). $^{13}$C NMR (126 MHz, DMSO) $\delta$ 165.03, 156.33, 150.18, 148.83, 147.45, 143.10, 133.65, 132.23, 131.17, 130.94, 130.68, 130.09, 129.31, 128.99, 125.78, 123.69, 120.20, 119.35, 114.09, 107.79, 100.94, 73.74, 52.61. HRMS (ESI-MS): calculated for $C_{28}H_{15}Br_4NO_7$ ($[M + H]^+$) = 793.7660 Da, found 793.7641 Da.

### Photophysical characterization instrumentation

All absorbance spectra were obtained on a Shimadzu UV-1800 UV Spectrophotometer and blanked with the respective solvent before measurements. Normalized spectra were obtained by normalizing to the $\lambda_{max}^{abs}$ of the respective compound. All fluorescence emission spectra and fluorescence time courses were obtained on a Shimadzu RF-6000 Spectrofluorophotometer. Quartz cuvettes with a 1.0 cm path length were used and purchased from Starna Scientific Ltd. Two LEDs, a 490 nm (M490L4) and a 530 nm (M530L3), were used for irradiation and were purchased from Thorlabs. The irradiation powers were determined using a Newport Optical Power meter Model 1916-R.

### Fluorescence quantum yield determination

Fluorescence quantum yields of **DB1** and **DB2** in PBS were measured using rhodamine B ($\Phi_f$ = 0.50 in ethanol)[30] as the reference standard and determined using the following equation:

$$\Phi_f^S = \Phi_f^R \left(\frac{n_S}{n_R}\right)^2 \left(\frac{I_S}{I_R}\right)\left(\frac{A_R}{A_S}\right)$$

where: S = sample, R = reference, $n$ = refractive index, $I$ = integrated fluorescence intensity, $A$ = absorbance, $\Phi$ = fluorescence quantum yield.

Subscripts s and r represent sample and reference standard, respectively.

Rhodamine B was measured in ethanol ($n$ = 1.36) while samples were measured in PBS ($n$ = 1.33). The absorbance of rhodamine B was taken at the maximal wavelength ($\lambda_{max}$) indicated in Table 1 to be 0.1 AU. Absorbance values of **DB1** and **DB2** were all $\leq$ 0.1 AU to avoid inner filter effects. Emission spectra of each sample with excitation at maximal wavelength (3 nm bandwidth) was taken with emission measured from $\lambda_{max}$ + 5 nm to 800 nm (1 nm emission bandwidth) at 1 nm s$^{-1}$ scan speed. Each emission spectra was integrated by Riemann sums at 1 nm intervals from $\lambda_{max}$ + 5 nm to 800 nm.

### $^1O_2$ Quantum yield determination (ABDA)

The absorbance of all compounds and the respective control, EY ($\Phi_\Delta$ = 0.50 in $H_2O$),[31] were matched at 490 nm to an absorbance of ~0.1 AU in PBS containing 2% DMSO. A 10 mM stock of ABDA was prepared in DMSO and diluted into the sample to an absorbance of ~0.3 AU at 401 nm. Absorbance at 401 nm was monitored over the irradiation period (490 nm, 28.0 mW cm$^{-2}$) to obtain the slopes of degradation of ABDA and calculate the singlet oxygen quantum yield using the following equation:

$$\Phi_\Delta^S = \Phi_\Delta^R \left(\frac{1-10^{-A_R}}{1-10^{-A_S}}\right)\left(\frac{m_S}{m_R}\right)$$

where: S = sample, R = reference, $A$ = absorbance, $m$ = slope of ABDA degradation.

The equation does not consider differences in refractive indexes or irradiation powers as the experiments were all conducted in MeOH with the same LED. All measurements were conducted in triplicate.

### Determination of extinction coefficients by qNMR

Compounds were dissolved in 392 μL DMSO-$d_6$ and 8 μL of a 500 μM stock of 1,4-dioxane in DMSO-$d_6$ was added. This provided a final concentration of 10 μM of 1,4-dioxane as the standard. The sample was then analyzed using a Bruker 400 MHz spectrometer and the ratio of the integrals of the chemical peaks was used to determine the concentration of the compound. UV-vis spectra were then obtained in anhydrous DMSO with a series of dilutions to generate a slope of the absorbance *vs.* concentration to determine the ε using Beer–Lambert Law ($A = \varepsilon lc$, where $l$ is 1 cm). All measurements were done in triplicate.

### NTR assay

Stocks of all compounds were kept in DMSO and all absorbance and fluorescence spectra were obtained at a final concentration of PBS (2% DMSO). Nitroreductase enzyme expressed in *E. coli* was purchased from Sigma-Aldrich and a final concentration of 200 μM NADH and 500 nM NTR was used for all experiments. Fluorescence time courses were obtained upon exciting at the $\lambda_{abs}$ and monitoring the $\lambda_{em}$ for **DB1** and **EY1** respectively.

 This journal is © The Royal Society of Chemistry 2025

Open Access Article. Published on 06 March 2025. Downloaded on 5/10/2026 2:26:02 AM. This article is licensed under a Creative Commons Attribution-NonCommercial 3.0 Unported Licence.

### Bacterial strains and preparation

Colonies of *E. coli* (N99 pXG10sf-GFP) and *B. subtilis* (wild-type) were thawed from frozen concentrated stocks. Bacteria were inoculated from an agar plate into 5 mL of LB broth (ampicillin and tetracycline antibiotics added to N99 *E. coli*) and grown at 37 °C overnight with shaking at 250 rpm. The next day, bacteria were regrown by diluting the overnight culture 100× into fresh LB broth (5 mL total volume) (antibiotics added for N99 *E. coli*). Bacteria were grown at 37 °C for an additional 2 hr with shaking at 250 rpm until they reached an exponential phase ($OD_{600}$ = 0.10–0.50). Standardized suspensions of bacteria were prepared for all experiments to the same $OD_{600}$.

### Fluorescent assay with bacteria

After the bacteria were cultured overnight and regrown, an initial $OD_{600}$ = 0.05 AU was used for fluorescent assays. Compound stocks in DMSO were added to the bacterial solution to a final concentration of 1 μM and contained a final concentration of 2% DMSO. Fluorescence was monitored by exciting the $\lambda_{abs}$ and monitoring the $\lambda_{em}$ of either **DB1** or **EY1** every 2 hours for the first 8 hours and one final timepoint at 24 hours. Bacteria were kept in the dark and at room temperature to prevent irradiation from ambient light and to minimize the growth of the bacteria. All measurements were conducted in triplicate.

### Cell viability *B. subtilis*

After culturing and regrowing *B. subtilis*, an initial $OD_{600}$ = 0.05 AU was used and incubated with a range of concentrations of **DB2** or **EY2** (0–3.2 μM) at room temperature for 4 hours and either left in the dark or irradiated with a 530 nm for 10 minutes (41.8 mW $cm^{-2}$). The $OD_{600}$ of the dark control (*B. subtilis* only) was measured to calculate the dilution factor required to reach a final $OD_{600}$ of $2.5 \times 10^{-4}$ for plating. All samples were diluted with LB broth and 5 μL of the diluted sample was spread using glass beads onto 6-well cell culture plates (35 mm diameter, cell star, cat. no. 657160) prepared previously by melting agarose (3 mL) and leaving to solidify at room temperature. Plates were left to incubate at 37 °C overnight before counting the colonies formed. Experiments were conducted in triplicate.

### Mammalian (HeLa and MRC-9) cell culture conditions

HeLa cells were cultured and maintained in a 75 $cm^2$ culture flask (Nunc™ EasYFlask™ 75 $cm^2$ Nunclon™ Delta Surface) at 37 °C and 5% $CO_2$ atmosphere in a Thermo Scientific Forma Steri-Cycle $CO_2$ Incubator. The cells were grown in Dulbecco's Modified Eagle Medium (DMEM) with sodium pyruvate, 4.5 g $L^{-1}$ glucose and L-glutamine (Wisent Inc.) supplemented with 10% fetal bovine serum and 1% antibiotics/antimycotics (complete growth medium).

MRC-9 cells were grown in minimum essential medium Eagle's (EMEM) with L-alanine, L-proline, L-serine, 1.5 g $L^{-1}$ sodium bicarbonate and sodium pyruvate, Earle's salts, L-glutamine, and glycine (Wisent Inc.) supplemented with 10% fetal bovine serum and 1% antibiotics/antimycotics (complete growth medium).

### Cell viability with DB1 or DB2 (MTT assay)

MRC-9 and HeLa cells were seeded at a density of 10 000 cells per well into 96-well plates (Thermo Scientific Nunclon™ Delta Surface) and incubated with 200 μL of EMEM or DMEM, respectively, overnight. The following day, the media was removed, and the cells were washed with D-PBS and replaced with 200 μL opti-minimal essential medium (Opti-MEM™, Thermo Scientific) containing 0 or 0.32 μM **DB2** and **DB1** to a final concentration of 2% DMSO. Plates were incubated at 37 °C for four hours, washed with D-PBS and the media was replaced with 200 μL of corresponding media. Plates were either kept in the dark or irradiated with a 530 nm LED for 10 minutes before incubating at 37 °C overnight. The following day, 20 μL of a 5 mg $mL^{-1}$ solution of thiazolyl blue tetrazolium bromide (MTT) in D-PBS was added to each well and incubated for 3 hours. The media was removed, and 150 μL DMSO was added to dissolve the formazan products. Plates were then read at 565 nm using a BioTek Synergy™ HTX multi-mode microplate reader. Absorbance values were then used to calculate the cell viability, and all viability experiments were conducted in triplicate.

## Data availability

The data supporting this article have been included as part of the ESI.†

## Conflicts of interest

The authors declare no competing financial interest.

## Acknowledgements

M. T. T. acknowledges support from the Ontario Graduate Scholarship and Queen Elizabeth II – Graduate Scholarship in Science and Technology. I. R. L.-M. acknowledges support from a Doctoral Research Award from Cancer Research Society (Grant 1330571) and a Queen Elizabeth II/Dina Gordon Malkin Graduate Scholarship in Science and Technology.

## Notes and references

1 J. O'Neill, Tackling drug-resistant infections globally: Final report and recommendations. HM Government and Wellcome Trust, London, 2016, **https://amr-review.org/sites/default/files/160518_Final%20paper_with%20cover.pdf** (accessed 2024-06-01).

2 T. C. Pham, V. N. Nguyen, Y. Choi, S. Lee and J. Yoon, Recent Strategies to Develop Innovative Photosensitizers for Enhanced Photodynamic Therapy, *Chem. Rev.*, 2021, **121**(21), 13454–13619, DOI: **10.1021/acs.chemrev.1c00381**.

3 Y. Y. Huang, S. K. Sharma, T. Dai, H. Chung, A. Yaroslavsky, M. Garcia-Diaz, J. Chang, L. Y. Chiang and M. R. Hamblin, Can

Open Access Article. Published on 06 March 2025. Downloaded on 5/10/2026 2:26:02 AM.
This article is licensed under a Creative Commons Attribution-NonCommercial 3.0 Unported Licence.

Nanotechnology Potentiate Photodynamic Therapy?, *Nanotechnol. Rev.*, 2012, **1**(2), 111–146, DOI: **10.1515/NTREV-2011-0005**.

4 J. H. Correia, J. A. Rodrigues, S. Pimenta, T. Dong and Z. Yang, Photodynamic Therapy Review: Principles, Photosensitizers, Applications, and Future Directions, *Pharmaceutics*, 2021, **13**(9), 1–16, DOI: **10.3390/pharmaceutics13091332**.

5 H. Mahmoudi, A. Bahador, M. Pourhajibagher and M. Y. Alikhani, Antimicrobial Photodynamic Therapy: An Effective Alternative Approach to Control Bacterial Infections, *J. Lasers Med. Sci.*, 2018, **9**(3), 154–160, DOI: **10.15171/JLMS.2018.29**.

6 Y. Liu, R. Qin, S. A. J. Zaat, E. Breukink and M. Heger, Antibacterial Photodynamic Therapy: Overview of a Promising Approach to Fight Antibiotic-Resistant Bacterial Infections, *J. Clin. Transl. Res.*, 2015, **1**(3), 140–167, DOI: **10.18053/jctres.201503.002**.

7 S. Rajesh, E. Koshi, K. Philip and A. Mohan, Antimicrobial Photodynamic Therapy: An Overview, *J. Indian Soc. Periodontol.*, 2011, **15**(4), 323–327, DOI: **10.4103/0972-124X.92563**.

8 R. B. Cecatto, L. S. Magalhaes, M. F. S. D. Rodrigues, C. Pavani, A. Lino-dos-Santos-Franco, M. T. Gomes and D. F. T. Silva, Methylene Blue Mediated Antimicrobial Photodynamic Therapy in Clinical Human Studies: The State of the Art, *Photodiagn. Photodyn. Ther.*, 2020, **31**, 101828, DOI: **10.1016/j.pdpdt.2020.101828**.

9 Y. Jao, S. J. Ding and C. C. Chen, Antimicrobial Photodynamic Therapy for the Treatment of Oral Infections: A Systematic Review, *J. Dent. Sci.*, 2023, **18**(4), 1453–1466, DOI: **10.1016/j.jds.2023.07.002**.

10 J. Ghorbani, D. Rahban, S. Aghamiri, A. Teymouri and A. Bahaador, Photosensitizers in Antibacterial Photodynamic Therapy: An Overview, *Laser Ther.*, 2018, **27**(4), 293–302, DOI: **10.5978/islsm.27_18-RA-01**.

11 M. Klausen, M. Ucuncu and M. Bradley, Design of Photosensitizing Agents for Targeted Antimicrobial Photodynamic Therapy, *Molecules*, 2020, **25**, 5239, DOI: **10.3390/molecules25225239**.

12 E. M. Digby, T. Ma, W. R. Zipfel, J. N. Milstein and A. A. Beharry, Highly Potent Photoinactivation of Bacteria Using a Water-Soluble, Cell-Permeable, DNA-Binding Photosensitizer, *ACS Infect. Dis.*, 2021, **7**(11), 3052–3061, DOI: **10.1021/acsinfecdis.1c00313**.

13 I. Nieves, C. Hally, C. Viappiani, M. Agut and S. Nonell, A Porphycene-Gentamicin Conjugate for Enhanced Photodynamic Inactivation of Bacteria, *Bioorg. Chem.*, 2020, **97**, 103661, DOI: **10.1016/J.BIOORG.2020.103661**.

14 G. Feng, Y. Yuan, H. Fang, R. Zhang, B. Xing, G. Zhang, D. Zhang and B. Liu, A Light-up Probe with Aggregation-Induced Emission Characteristics (AIE) for Selective Imaging, Naked-Eye Detection and Photodynamic Killing of Gram-Positive Bacteria, *Chem. Commun.*, 2015, **51**, 12490, DOI: **10.1039/c5cc03807c**.

15 L. Huang, M. Wang, Y. Y. Huang, A. El-Hussein, L. M. Wolf, L. Y. Chiang and M. R. Hamblin, Progressive Cationic Functionalization of Chlorin Derivatives for Antimicrobial Photodynamic Inactivation and Related Vancomycin Conjugates, *Photochem. Photobiol. Sci.*, 2018, **17**, 638, DOI: **10.1039/c7pp00389g**.

16 R. C. C. de Pietra, R. C. Cruz, C. N. Melo, L. B. Rodrigues, P. C. Santos, G. P. M. Bretz, B. M. Soares, G. R. de Sousa, M. V. L. Ferreira, P. S. Cisalpino, P. P. Magalhães, L. de M. Farias and M. Pinotti, Evaluation of Polymeric PLGA Nanoparticles Conjugated to Curcumin for Use in APDT, *Braz. J. Pharm. Sci.*, 2017, **53**(2), e16043, DOI: **10.1590/S2175-97902017000216043**.

17 V. Klepac-Ceraj, N. Patel, X. Song, C. Holewa, C. Patel, R. Kent, M. M. Amiji and N. S. Soukos, Photodynamic Effects of Methylene Blue-Loaded Polymeric Nanoparticles on Dental Plaque Bacteria, *Lasers Surg. Med.*, 2011, **43**(7), 600–606, DOI: **10.1002/LSM.21069**.

18 G. S. De Paula, M. C. Oliveira, L. S. Sales, M. Boriollo, L. K. A. Rodrigues, M. Nobre-dos-Santos and C. Steiner-Oliveira, Antimicrobial Photodynamic Therapy Mediated by Methylene Blue Complex to β-Cyclodextrin Reduces Early Colonizing Microorganisms from the Oral Biofilm, *Photodiagn. Photodyn. Ther.*, 2021, **34**, 102283, DOI: **10.1016/j.pdpdt.2021.102283**.

19 G. A. Johnson, E. A. Ellis, H. Kim, N. Muthukrishnan, T. Snavely and J. P. Pellois, Photoinduced Membrane Damage of E. Coli and S. Aureus by the Photosensitizer-Antimicrobial Peptide Conjugate Eosin-(KLAKLAK)2, *PLoS One*, 2014, **9**(3), e91220, DOI: **10.1371/JOURNAL.PONE.0091220**.

20 K. Yang, B. Gitter, R. Rüger, G. D. Wieland, M. Chen, X. Liu, V. Albrecht and A. Fahr, Antimicrobial Peptide-Modified Liposomes for Bacteria Targeted Delivery of Temoporfin in Photodynamic Antimicrobial Chemotherapy, *Photochem. Photobiol. Sci.*, 2011, **10**, 1593–1601, DOI: **10.1039/C1PP05100H**.

21 Z. Li, Q. Feng and J. Shen, A β-Lactamase-Activatable Photosensitizer for the Treatment of Resistant Bacterial Infections, *Chin. Chem. Lett.*, 2024, **35**(11), 109602, DOI: **10.1016/J.CCLET.2024.109602**.

22 W. Zhou, X. Da, Y. Jian, Y. Peng, X. Liu, Y. Xu, Y. Wu, X. Wang and Q. Zhou, Nitroreductase-Responsive Photosensitizers for Selective Imaging and Photo-Inactivation of Intracellular Bacteria, *Chem. – Eur. J.*, 2024, **30**(16), e202303766, DOI: **10.1002/CHEM.202303766**.

23 M. D. Roldán, E. Pérez-Reinado, F. Castillo and C. Moreno-Vivián, Reduction of Polynitroaromatic Compounds: The Bacterial Nitroreductases, *FEMS Microbiol. Rev.*, 2008, **32**(3), 474–500, DOI: **10.1111/J.1574-6976.2008.00107.x**.

24 H. A. J. Hibbard and M. M. Reynolds, Synthesis of Novel Nitroreductase Enzyme-Activated Nitric Oxide Prodrugs to Site-Specifically Kill Bacteria, *Bioorg. Chem.*, 2019, **93**, 103318, DOI: **10.1016/J.BIOORG.2019.103318**.

25 K. A. Pardeshi, T. A. Kumar, G. Ravikumar, M. Shukla, G. Kaul, S. Chopra and H. Chakrapani, Targeted Antibacterial Activity Guided by Bacteria-Specific Nitroreductase Catalytic Activation to Produce Ciprofloxacin, *Bioconjugate Chem.*, 2019, **30**(3), 751–759, DOI: **10.1021/ACS.BIOCONJCHEM.8B00887**.

26 S. Jiao, S. Yang, X. Meng and C. Wang, One Step Synthesis of Red-Emitting Fluorescence Turn-on Probe for Nitroreductase and Its Application to Bacterial Detection and Oral Cancer Cell Imaging, *Spectrochim. Acta, Part A*, 2020, **241**, 118637, DOI: **10.1016/J.SAA.2020.118637**.

 This journal is © The Royal Society of Chemistry 2025

Open Access Article. Published on 06 March 2025. Downloaded on 5/10/2026 2:26:02 AM.
This article is licensed under a Creative Commons Attribution-NonCommercial 3.0 Unported Licence.

27 J. W. Yoon, S. Kim, Y. Yoon and M. H. Lee, A Resorufin-Based Fluorescent Turn-on Probe Responsive to Nitroreductase Activity and Its Application to Bacterial Detection, *Dyes Pigm.*, 2019, **171**, 107779, DOI: **10.1016/J.DYEPIG.2019.107779**.

28 F. Xu, H. Li, Q. Yao, H. Ge, J. Fan, W. Sun, J. Wang and X. Peng, Hypoxia-Activated NIR Photosensitizer Anchoring in the Mitochondria for Photodynamic Therapy, *Chem. Sci.*, 2019, **10**(45), 10586–10594, DOI: **10.1039/C9SC03355F**.

29 Z. Liu, F. Song, W. Shi, G. Gurzadyan, H. Yin, B. Song, R. Liang and X. Peng, Nitroreductase-Activatable Theranostic Molecules with High PDT Efficiency under Mild Hypoxia Based on a TADF Fluorescein Derivative, *ACS Appl. Mater. Interfaces*, 2019, **11**(17), 15426–15435, DOI: **10.1021/ACSAMI.9B04488**.

30 T. Karstens and K. Kobs, Rhodamine B and Rhodamine 101 as Reference Substances for Fluorescence Quantum Yield Measurements, *J. Phys. Chem.*, 1980, **84**, 1871–1872, DOI: **10.1021/j100451a030**.

31 R. W. Redmond and J. N. Gamlin, A Compilation of Singlet Oxygen Yields from Biologically Relevant Molecules, *Photochem. Photobiol.*, 1999, **70**(4), 391–475, DOI: **10.1111/J.1751-1097.1999.TB08240.X**.

32 C. Maher and K. A. Hassan, The Gram-Negative Permeability Barrier: Tipping the Balance of the in and the out, *MBio*, 2023, **14**(6), e01205, DOI: **10.1128/MBIO.01205-23**.

33 E. H. H. Wong, M. M. Khin, V. Ravikumar, Z. Si, S. A. Rice and M. B. Chan-Park, Modulating Antimicrobial Activity and Mammalian Cell Biocompatibility with Glucosamine-Functionalized Star Polymers, *Biomacromolecules*, 2016, **17**, 1170–1178, DOI: **10.1021/ACS.BIOMAC.5B01766**.

34 G. Y. C. Cheung, J. S. Bae and M. Otto, Pathogenicity and Virulence of Staphylococcus Aureus, *Virulence*, 2021, **12**(1), 547–569, DOI: **10.1080/21505594.2021.1878688**.

35 S. Y. C. Tong, J. S. Davis, E. Eichenberger, T. L. Holland and V. G. Fowler, Staphylococcus Aureus Infections: Epidemiology, Pathophysiology, Clinical Manifestations, and Management, *Clin. Microbiol. Rev.*, 2015, **28**(3), 603–661, DOI: **10.1128/CMR.00134-14**.

36 A. Zhao, J. Sun and Y. Liu, Understanding Bacterial Biofilms: From Definition to Treatment Strategies, *Front. Cell. Infect. Microbiol.*, 2023, **13**, 1137947, DOI: **10.3389/FCIMB.2023.1137947/BIBTEX**.

37 H. K. N. Vyas, B. Xia and A. Mai-Prochnow, Clinically Relevant in Vitro Biofilm Models: A Need to Mimic and Recapitulate the Host Environment, *Biofilm*, 2022, **4**, 100069, DOI: **10.1016/J.BIOFLM.2022.100069**.

38 T. D. Gruber, C. Krishnamurthy, J. B. Grimm, M. R. Tadross, L. M. Wysocki, Z. J. Gartner and L. D. Lavis, Cell-Specific Chemical Delivery Using a Selective Nitroreductase-Nitroaryl Pair, *ACS Chem. Biol.*, 2018, **13**(10), 2888–2896, DOI: **10.1021/ACSCHEMBIO.8B00524**.